Green Chemistry

PAPER

View Article Online
View Journal

Cite this: DOI: 10.1039/d6gc00467a

De novo microbial production of picolinic acid *via* a short-cut biosynthetic pathway

Cui Guo, [a] Ashley Tseng, [a] Nguyen N. T. Luu[a] and Yuheng Lin *[a,b]

Picolinic acid (PA) is a tryptophan-derived metabolite produced in animals *via* the kynurenine pathway. Its strong metal-chelating properties and broad antimicrobial, antiviral, and anticancer activities have driven widespread use of PA salts in nutritional supplements and animal feed. Current industrial PA manufacturing depends on petroleum-derived substrates and harsh chemical processes, generating significant environmental burdens. In this work, we develop a sustainable microbial alternative by engineering an artificial shortcut pathway in *Escherichia coli*. Using chorismate as the entry point, we constructed a hybrid route that couples salicylic acid (SA) biosynthesis with a partial SA degradation module, enabling PA formation in only four enzymatic steps, far fewer than the eleven-step natural pathway. Enhancing SA precursor flux through a pyruvate-mediated metabolic driving force, together with fermentation optimization, allowed the engineered strain to produce 560.02 mg L^{-1} PA in shake-flask cultures from glucose. This work presents an innovative biocatalytic strategy for PA production and underscores the commercial promise of a biotechnological route capable of replacing conventional chemical synthesis and advancing sustainable PA manufacturing.

Received 23rd January 2026,
Accepted 27th April 2026

DOI: 10.1039/d6gc00467a

rsc.li/greenchem

Green foundation

1. Designed, constructed, and optimized an artificial biosynthetic pathway in *Escherichia coli* for efficient picolinic acid (PA) production from renewable carbon sources.
2. The engineered pathway employs only four enzymatic steps and shortens the natural biosynthetic route by seven steps, enabling a simplified biocatalytic process with higher yield.
3. Continued metabolic and process optimization is expected to further increase titer, yield, and productivity, while enabling the use of a wider range of renewable feedstocks for PA production.

Introduction

Picolinic acid (PA) is a tryptophan-derived metabolite produced in mammals *via* the kynurenine pathway.[1,2] Its broad biological activities arise largely from its strong affinity for divalent and trivalent metal ions. By coordinating metals such as Cr^{3+}, Zn^{2+}, Fe^{2+}, Cu^{2+}, and Mn^{2+} through its pyridine nitrogen and carboxylate oxygen atoms, PA forms stable complexes that influence metal uptake, intracellular distribution, and redox behaviour in biological systems.[3,4] These interactions enhance intestinal absorption of poorly soluble metals, modulate immune and inflammatory responses, and suppress oxidative stress by sequestering redox-active iron and copper.[5–10] Beyond metal homeostasis, PA also limits the formation of the neurotoxin quinolinic acid (QA), provides neuroprotective benefits,[2] and exhibits antimicrobial and antiviral activities, such as inhibiting *Mycobacterium avium*,[11] and blocking entry of enveloped viruses including SARS-CoV-2 and influenza A.[12] The physiological and commercial relevance of PA and its metal salts have stimulated growing interest in expanding their applications across nutritional, biomedical, and agricultural sectors.

Rising demand for PA has renewed attention on its production methods. Current industrial manufacturing relies primarily on chemical oxidation routes, including the ammoxidation of 2-picoline or nitric acid-based oxidation, which require harsh conditions, hazardous reagents, and generate substantial waste, ultimately imposing considerable environmental burdens and motivating the search for greener, more sustainable production strategies.[13]

Microbial biosynthesis offers a compelling and sustainable alternative, particularly as advances in synthetic biology and metabolic engineering have enabled the scalable production of

[a]*Biotechnology Program, Department of Engineering Technology, Cullen College of Engineering, University of Houston, Sugar Land, Texas 77479, USA*
[b]*Department of Biomedical Engineering, Cullen College of Engineering, University of Houston, Sugar Land, Texas 77479, USA. E-mail: ylin70@uh.edu*

numerous value-added chemicals from renewable carbon sources.[14–17] However, PA production has not yet benefited from such biotechnological development to date. No effective microbial cell factories have been reported for producing PA from renewables. Although the natural PA biosynthesis pathway is well characterized, it is rarely exploited for engineered microbial production due to some intrinsic challenges. First, PA is only a minor branch product of tryptophan degradation. In the kynurenine pathway (Fig. 1), tryptophan is sequentially converted to *N*-formylkynurenine, kynurenine, 3-hydroxy-kynurenine (3-HK) and 3-hydroxy-anthranilic acid (3-HAA). Oxidative ring cleavage of 3-HAA yields 2-amino-3-carboxymuconate semialdehyde (ACMS), which predominantly cyclizes spontaneously to QA, the precursor of NAD^+.[18] Only a small fraction of ACMS undergoes decarboxylation to 2-aminomuconate semialdehyde (AMS), which then non-enzymatically cyclizes to PA.[2] Moreover, reconstructing this natural route in a microbial host would require linking the tryptophan biosynthesis pathway to its downstream catabolic steps, involving a total of 11 enzymes and 12 reactions from the shikimate pathway intermediate chorismate. This pathway length, complexity, and the strong intrinsic flux toward QA make engineering efforts inefficient and severely limit PA accumulation.

To overcome these constraints, we designed and established an artificial shortcut pathway for PA biosynthesis through a retro-biosynthetic strategy, which bypasses the kynurenine pathway. This engineered route extends the shikimate pathway by integrating a hybrid salicylic acid (SA) biosynthetic module with a partial SA degradation pathway, comprising only four enzymatic steps from chorismate and shortening the natural route by seven steps. In this design, SA derived from chorismate is converted to PA *via* catechol through the sequential activities of salicylate hydroxylase (NahG) and catechol 2,3-dioxygenase (CbzE). The resulting intermediate 2-hydroxymuconate-6-semialdehyde (HMS) is spontaneously converted to PA in the presence of ammonium (NH^{4+}). Through enzyme validation, pathway assembly in *Escherichia coli*, and optimization of gene expression, precursor supply,

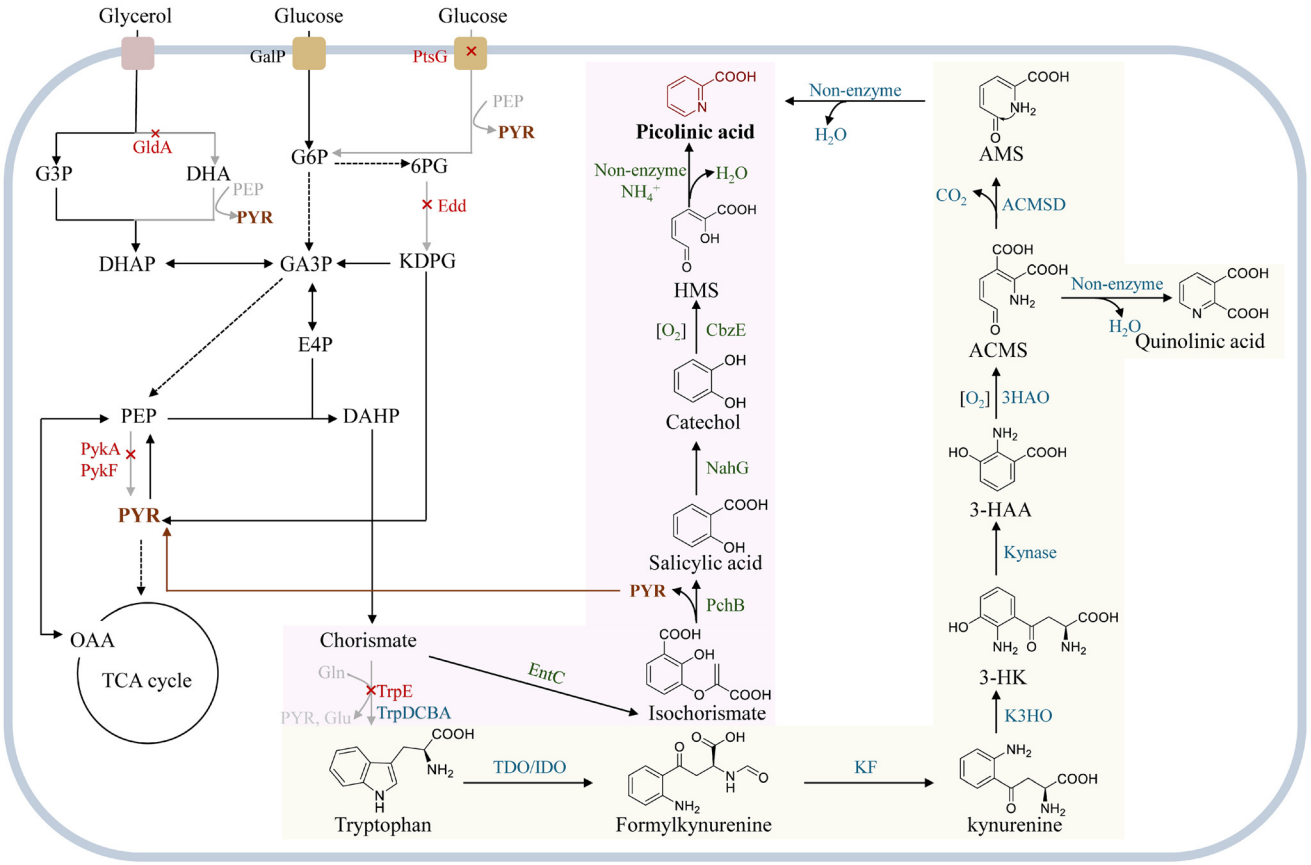

Fig. 1 Artificial short-cut PA biosynthetic pathway in *E. coli* (pink) and natural PA biosynthetic pathway in animal (yellow). G3P: glycerol 3-phosphate; DHA: dihydroxyacetone; DHAP: dihydroxyacetone phosphate; G6P: glucose-6-phosphate; GA3P: glyceraldehyde-3-phosphate; 6-PG: 6-phosphogluconate; KDPG: 2-keto-3-deoxy-6-phosphogluconate; E4P: D-erythrose 4-phosphate; PEP: phosphoenolpyruvate; DAHP, 3-deoxy-D-arabinoheptulosonate 7-phosphate; PYR: pyruvate; AMS: 2-amino-muconate-6-semialdehyde; 3-HK: 3-hydroxy-kynurenine; 3-HAA: 3-hydroxy-anthranilic acid; ACMS: 2-amino-3-carboxymuconate-6-semialdehyde; GldA: glycerol dehydrogenase; PtsG: PTS system glucose-specific EIICB component; PykA: pyruvate kinase II; PykF: pyruvate kinase I; TrpE: anthranilate synthase; Edd: phosphogluconate dehydratase; EntC: isochorismate synthase; PchB: isochorismate pyruvate lyase; NahG: salicylate hydroxylase; CbzE: catechol 2,3-dioxygenase; HMS: 2-hydroxymuconate-6-semialdehyde; IDO: indoleamine-2,3-dioxygenase; TDO: tryptophan 2,3-dioxygenase; KF: kynurenine aminotransferase; K3HO: kynurenine-3-hydroxylase; Kynase: kynureninease; 3HAO: 3-hydroxyanthranilic acid oxygenase; ACMSD: 2-amino-3-carboxymuconate-semialdehyde decarboxylase.

and cultivation conditions, we achieved *de novo* PA production from glucose and glycerol. The engineered strain produced up to 560.02 ± 5.75 mg L^{-1} PA from glucose in shake-flask cultures. This artificial biosynthetic pathway provides a novel and foundational platform for sustainable and scalable PA production to meet growing market demand.

Experimental

Experimental material

Luria–Bertani (LB) medium containing 10 g L^{-1} tryptone, 5 g L^{-1} yeast extract, and 10 g L^{-1} NaCl was used to culture *E. coli* for plasmid construction and inoculum preparation. M9Y medium (per liter) consisting of 15 g of glycerol or glucose, 8 g yeast extract, 11.28 g 5 × M9 salts, 3 g $(NH_4)_2SO_4$, 2 g trisodium citrate, 1 mM $MgSO_4$, 0.1 mM $CaCl_2$, 10 mg vitamin B1 was used for feeding experiments and *de novo* production of PA. The respective antibiotics ampicillin (100 mg L^{-1}), kanamycin (50 mg L^{-1}), chloramphenicol (34 mg L^{-1}), and spectinomycin (50 mg L^{-1}) were added to culture media when necessary. pCas and pTargetF purchased from Addgene (62225 and 62226, respectively) were used for knockout genes. SA, catechol, and PA were purchased from Thermo Fisher Scientific.

Strains and construction of plasmids

Strains and plasmids used in this study are listed in Table S1. *E. coli* XL1-blue was used as host strain for plasmids cloning and propagation. *E. coli* BW25113 (F′) and pyruvate-deficient strains including glucose-utilizing strains: AT1 to AT6 and glycerol-utilizing strains: AT7 and AT8 were used as host stains for feeding experiments and production of SA and PA. The plasmids pHA-GFP, pMK-GFP, and pLC-GFP were used as high-, medium-, and low-copy backbones for plasmid construction, respectively.[14] The plasmid pLC-NahG was constructed by inserting synthetic gene *nahG* into pLC-GFP using restriction enzyme sites Acc65I and SalI. The gene *cbzE* was synthesized and then subcloned into pHA vector using Acc65I and SalI, yielding plasmid pHA-CbzE. The gene *entC* was amplified from *E. coli* genomic DNA, and *pchB* was synthesized. The plasmid pHA-EP was constructed through ligation of two DNA fragments entC/pchB with vector pHA-GFP with restriction enzyme sites Acc65I, NdeI, and SalI.

The plasmid pMK-LPTG was constructed in our previous study.[14] The gene *cbzE* was sub-cloned into pHA-EP and pLC-NahG, using restriction enzyme sites BamHI/ApaI and SalI/BamHI, respectively, generating plasmids pHA-EP-CbzE and pLC-NahG-CbzE. The expression vector pMK-LPTG-CbzE was constructed by introducing the expression operon $P_L$lacO1-CbzE into pMK-LPTG. pTargetF variants were assembled by digesting the respective N20 sequences with SpeI and XhoI and inserted into pTargetF.

Gene disruption

Gene knockouts to *E. coli* BW25113 (F′) genome were conducted using CRISPR-Cas9 based genome edition tools as previously described.[19] Donor DNA was constructed using primers (Table S2) which yielded upstream and downstream fragments, which were combined into a singular fragment using overlap PCR. Knockout strains were confirmed by colony PCR.

Feeding experiments

Feeding experiments were conducted to validate *in vivo* activities of NahG and CbzE by examining the production of catechol from SA and PA from catechol. *E. coli* BW25113 (F′) was transformed with the plasmids pLC-NahG and pHA-CbzE, respectively. Randomly picked single colonies were inoculated into 4 mL LB medium containing appropriate antibiotic and incubated at 37 °C with shaking at 220 rpm for 16 h. Then, 1 mL of overnight cultures were inoculated into 20 mL M9Y medium with appropriate antibiotic in 125 mL baffled shaking flasks and then incubated at 37 °C with shaking at 300 rpm, fed with 0.1 mM $FeSO_4$. After 3 h of incubation, the cultures were fed with 0.5 mM IPTG. After 6 h of incubation, 15 g L^{-1} glycerol and appropriate substrates (1 g L^{-1} SA or 2 g L^{-1} catechol) were fed into the cultures, then the temperature was changed to 30 °C. Samples were taken at 24, 30, and 48 h following inoculation. OD600 was measured to assess cell density. Product concentrations were analyzed *via* HPLC. Samples were prepared for HPLC analysis by centrifuging at 14 000 rpm in 10 min.

De novo production of SA and PA

For *de novo* production of SA, the plasmids pHA-EP and pMK-LPTG were co-transformed into BW25113 (F′) and knockout strains using heat shock or electro transformation. Single colonies were inoculated and incubated in LB media with the respective antibiotic(s) for 16 hours. 1 mL of seed culture was transferred into 20 mL of M9Y media with the respective carbon source. The flasks were incubated in a shaking incubator at 37 °C at 300 rpm, fed with 0.5 mM IPTG, 0.1 mM $FeSO_4$. Samples were taken at 24, 30, and 48 h following inoculation.

For *de novo* biosynthesis of PA, overnight LB cultures of the producing strains were inoculated into the M9Y medium containing appropriated antibiotics and then incubated at 37 °C with shaking at 300 rpm. For testing ammonium contribution, different concentrations of ammonium at 40, 60, 80, 100, 150, and 200 mM were added into medium. IPTG was added at 3 h after inoculation (0.5 mM). For optimization, IPTG concentrations of 0, 0.1, 0.2, 0.5, 0.8, and 1.0 mM were tested. After a total of 6 h of incubation, additional glucose or glycerol (15 g L^{-1}) was added. The inoculation temperature was then changed to 30 °C. For optimization, the temperatures 30 and 37 °C were tested. Samples were collected at 24, 30, and 48 h following inoculation. OD600 was measured to assess cell density. Product concentrations were analyzed *via* HPLC.

Chromatography analysis

Quantification of SA, catechol, and PA were performed by Shimadzu HPLC LC-2050c series (Shimadzu, Kyoto, Japan) with a PDA detector (applied range: 190–800 nm) using an Agilent reverse-phase Zorbax SB-C18 column (250 mm ×

4.6 mm, 5 μm, Agilent Technologies, Santa Clara, America), maintained at 28 or 20 °C during analyses. The mobile phase was composed of water (solvent A) containing 0.05% trifluoroacetic acid (TFA), and pure methanol (solvent B), delivered at 1.0 mL min^{-1} with the gradient of B phase as follows for catechol and PA: 5–60% (0–15 min), 60–5% (15–16 min), 5% (16–20 min). For SA, the mobile phase consisted of water containing 0.1% trifluoroacetic acid (solvent A) and methanol (solvent B). The flow rate was set at 1 mL min^{-1} with the column held at 28 °C. The elution gradient was set as: solvent B concentration 10–70% for 0–15 min, 70–10% for 1 min and 10% for 4 min. The quantification of SA, catechol, and PA were conducted based on the peak area analyzed at 303, 275, and 260 nm, respectively. The retention times of SA, catechol, and PA were 16.225, 11.339, and 4.093 min.

Results and discussion

Retro-biosynthetic design of an artificial PA biosynthetic pathway

Only a single biosynthetic route to picolinic acid (PA) is known in nature to date. In mammals, PA is generated from exogenous tryptophan *via* the seven-step kynurenine pathway, which consists of six enzymatic reactions followed by a non-enzymatic cyclization (Fig. 1). Reconstructing this pathway in microbes for *de novo* PA production would require incorporating a five-step tryptophan biosynthetic module, resulting in an even longer 12-step route originating from chorismate. This lengthy route introduces substantial complexity, making pathway construction and optimization highly challenging. In addition, the key intermediate ACMS undergoes rapid spontaneous cyclization to QA,[20] diverting metabolic flux away from PA and severely limiting attainable titer and yield.

To circumvent these limitations, we designed an artificial shortcut pathway for PA biosynthesis using a retro-biosynthetic strategy. This design was inspired by a reported catechol degradation route in which PA is formed *via* a catechol ring-cleavage reaction catalysed by catechol 2,3-dioxygenase, followed by spontaneous conversion of the ring-fission product HMS in the presence of ammonium.[21] Working backward from this chemistry, we sought enzymatic steps capable of generating catechol from a metabolite with high flux in *E. coli*. In our previous work, we established a biosynthetic pathway that converts the shikimate-derived intermediate chorismate to muconic acid through SA and catechol.[22] In this pathway, chorismate is converted to catechol through the sequential actions of isochorismate synthase (ICS from *E. coli*), isochorismate pyruvate lyase (IPL from *Pseudomonas fluorescens* Migula) and salicylate 1-monoxyganase (SMO from *P. putida*). By integrating this catechol biosynthesis module with a catechol-to-PA conversion step, we designed an artificial short-cut pathway comprising only four enzymatic reactions from chorismate (Fig. 1), which is expected to enable *de novo* PA production from renewable carbon sources.

Validating the bioconversion of catechol to PA

The terminal step in PA biosynthesis is the conversion of catechol into PA through two reactions. First, catechol 2,3-dioxygenase cleaves the C2–C3 bond of catechol in a dioxygenation reaction to yield HMS. Subsequently, HMS undergoes non-enzymatic cyclization in the presence of ammonium to yield PA.[21] Catechol 2,3-dioxygenases, as key aromatic ring-cleaving enzymes, play a central role in catechol degradation and are therefore widespread in microorganisms, particularly soil bacteria such as *Pseudomonas* sp.,[23,24] *Brevibacterium fuscum*,[25,26] *Bacillus ligniniphilus*,[27] *Arthrobacter globiformis*.[28] Among these, we selected CbzE (GenBank: AF109307.1) from *P. putida* GJ31, which belongs to the 2.C subfamily of type I extradiol dioxygenases, due to its reported high activity, resistance to suicide inactivation and lower susceptibility to inhibition by methylated catechols.[23,29]

To evaluate CbzE activity in *E. coli*, the *cbzE* gene was synthesized and cloned into the high-copy plasmid pHA-GFP, generating pHA-CbzE. This construct was then introduced into BW25113 (F′) strain, yielding the recombinant strain PABW01. To facilitate the non-enzymatic cyclization of HMS to PA, the ammonium concentration in medium was set to 200 mM and pH was adjusted to 7.0. When incubated with 2 g L^{-1} of catechol (18.16 mM), PABW02 produced 1265.97 ± 45.41 mg L^{-1} (10.28 mM) of PA within 24 h, completely consuming the supplied precursor catechol, corresponding to a molar yield of 56.61% (Fig. 2A and B). The observed sub-stoichiometric conversion is attributed to the inherent chemical instability of the reactive intermediate, HMS, which is prone to decomposition even during storage at −20 °C.[21]

Bioconversion of SA to catechol

SMO catalyses the first committed enzymatic step in SA degradation, leading to the production of catechol. Securing an efficient SMO is critical for assembling a functional and pro-

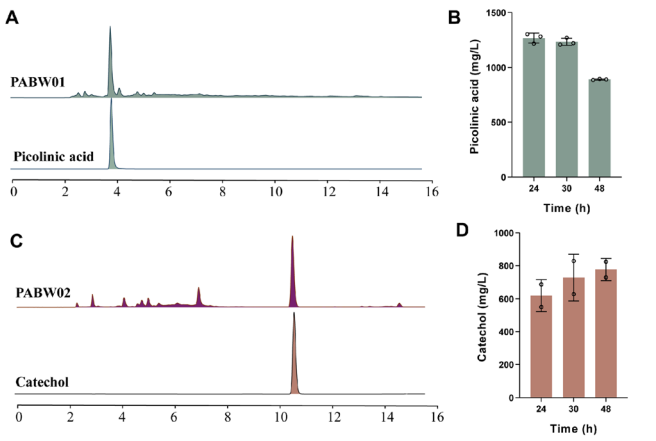

Fig. 2 Validation of enzymes of CbzE and NahG activity *in vivo*. (A) HPLC analysis of strain PABW01 and commercial PA standard. (B) PA titer of strain PABW01. (C) HPLC analysis of strain PABW02 and standard catechol. (D) Catechol titer of strain PABW02. All data points are reported as mean ± standard deviation from at least two replicates.

ductive pathway. An efficient SMO (encoded by *nahG*) from the genome of *P. putida* DOT-T1E, had been previously characterized to efficiently convert SA to catechol *via* a decarboxylative hydroxylation reaction.[22] Given the prior report indicating that relatively low expression of the NahG was more beneficial for converting SA in *E. coli*,[22] we cloned the *nahG* gene into a low-copy-number plasmid pLC-GFP, generating the expression vector pLC-NahG for *in vivo* assay.

The engineered strain PABW02 harbouring plasmid pLC-NahG was cultivated and supplied with 1 g L^{-1} (7.24 mM) SA. After 48 h, the strain PABW02 produced 776.90 ± 66.84 mg L^{-1} of catechol (7.06 mM), with 86.13 mg L^{-1} of precursor SA left unconverted, corresponding to a molar conversion yield of 106.65% from consumed SA (Fig. 2C and D, and S1). The slightly supra-stoichiometric yield is likely attributable to minor evaporation of cell culture during the extended cultivation. The results conclusively demonstrate that NahG possesses strong decarboxylative hydroxylation activity towards SA *in vivo*.

Optimization of SA biosynthesis through a pyruvate-based metabolic driving force

Following the validation of NahG and CbzE, we next sought to optimize the SA biosynthesis module, as achieving high metabolic flux toward SA is essential for maximizing PA production. To accomplish this, we adopted an established strategy that leverages a pyruvate-mediated metabolic driving force. In this approach, a pyruvate-deficient host with impaired growth is constructed by deleting key genes involved in pyruvate formation. Introducing a heterologous biosynthetic pathway that generates pyruvate as a byproduct can then restore growth, effectively coupling cell proliferation with product formation and thereby improving both titer and yield.[30,31] Notably, the SA biosynthesis pathway catalysed by ICS and IPL intrinsically releases pyruvate as a co-product,[22,32] making it inherently well suited for establishing this growth-coupled metabolic driving force (Fig. 3A).

To create an effective pyruvate-deficient host strain, we inactivated endogenous pyruvate-generating genes individually and in various combinations in *E. coli* BW25113 (F′). In *E coli*, pyruvate is primarily produced through pyruvate kinases and the phosphotransferase systems (PTS) for glucose and mannose. Firstly, the pyruvate kinase genes *pykA* and *pykF* were inactivated, resulting in strain AT1 (Δ*pykA*Δ*pykF*, Table S1).[33] Building on AT1, further inactivation of the glucose PTS (PtsG) alone or in combination of concurrent inactivation of mannose PTS (ManXYZ)[34] led to strain AT2 (Δ*pykA*Δ*pykF*Δ*ptsG*) and AT5 (Δ*pykA*Δ*pykF*Δ*ptsG*Δ*manXYZ*), respectively.[35] We next examined the contribution of minor pyruvate-generating reactions. The first committed step of tryptophan biosynthesis, catalyzed by TrpE, generates pyruvate as a side product.[36] Inactivation of *trpE* in AT2 and AT5 led to the creation of AT3 (Δ*pykA*Δ*pykF*Δ*ptsG*Δ*trpE*) and AT6 (Δ*pykA*Δ*pykF*Δ*ptsG*Δ*manXYZ* Δ*trpE*), respectively. Additionally, *edd*, which encodes 6-phosphogluconate (6-PG) dehydratase and converts 6-PG into pyruvate and GAP[37] was deleted from AT3 to generate strain AT4 (Δ*pykA*Δ*pykF*Δ*ptsG*Δ*trpE*Δ*edd*) (Table S1).

To evaluate SA production in these pyruvate-deficient strains, *entC* from *E. coli* BW25113 and *pchB* from *P. fluorescens* were cloned into a high-copy plasmid (pHA-GFP), resulting in pHA-EP (Fig. 3A and B). As shown in Fig. 3C, the parental strain BW25113 (F′) harboring pHA-EP produced only 49.57 ± 0.47 mg L^{-1} SA at 48 h. Among the glucose-utilizing pyruvate-driven strains, AT3 achieved the highest SA titer, producing 1229.01 ± 84.31 mg L^{-1} at 48 h when no tryptophan is supplemented in the culture (Fig. 3C), a 24.79-fold increase over BW25113 (F′). In contrast, supplementing tryptophan in the culture reduced the SA titer, likely due to pathway feedback inhibition that resulted in less metabolic flux.[38] Given its superior performance, AT3 was selected for subsequent experiments.

We next constructed pyruvate-deficient strains optimized for glycerol utilization. Deletion of *gldA* in AT1 prevented carbon flux from entering the gldA-dhaKLM-mediated pyruvate-generating pathway, resulting in strain AT7. Subsequent deletion of *trpE* yielded strain AT8 (Table S1). When assessing SA production from glycerol, wild-type BW25113 (F′) carrying pHA-EP again produced the lowest titer (149.49 ± 4.19 mg L^{-1}). In comparison, AT8 (Δ*pykA*Δ*pyk*Δ*gldA* Δ*trpE*) carrying the same plasmid produced 1222.27 ± 40.02 mg L^{-1} SA, representing an 8.18-fold improvement over BW25113 (F′) (Fig. 3D). Supplementing tryptophan increased cell density (Fig. S2) but reduced SA titer relative to unsupplemented AT8 cultures (Fig. 3D).

Elevation of SA production *via* precursor boosting

To further enhance SA production, we reasoned that increasing carbon flux into the shikimate pathway by overexpressing key rate-limiting enzymes would promote the accumulation of the precursor chorismate. Following a previously established strategy, we introduced the LPTG expression module, comprising *aroL*, *ppsA*, *tktA*, and $aroG^{fbr}$, a feedback-inhibition-resistant mutant of *aroG*, into the medium-copy plasmid pMK-GFP to generate pMK-LPTG,[14] which was subsequently co-transformed with pHA-EP (Fig. 3E).

Co-expression of pHA-EP and pMK-LPTG in strain AT3 resulted in the accumulation of 2991.75 ± 58.07 mg L^{-1} SA from glucose at 48 h, representing a 14.72-fold increase relative to BW25113 (F′) (203.28 ± 6.21 mg L^{-1}) (Fig. 3F) and a 2.43-fold improvement over AT3 expressing only pHA-EP (Fig. 3C). Similarly, when cultivated on glycerol, both BW25113 (F′) and AT8 carrying pHA-EP and pMK-LPTG also exhibited elevated SA titers compared to the corresponding strains without pMK-LPTG. AT8 accumulated 3088.50 ± 42.18 mg L^{-1} at 48 h, corresponding to a 4.52-fold increase over BW25113 (F′) (Fig. 3G) and a 2.53-fold improvement compared to AT8 harboring only pHA-EP (Fig. 3D).

These results demonstrate that overexpression of *aroL*, *ppsA*, *tktA*, and feedback-inhibition-resistant *aroG* effectively redirected carbon flux toward SA biosynthesis, substantially enhancing production in wildtype and pyruvate-driven knockout

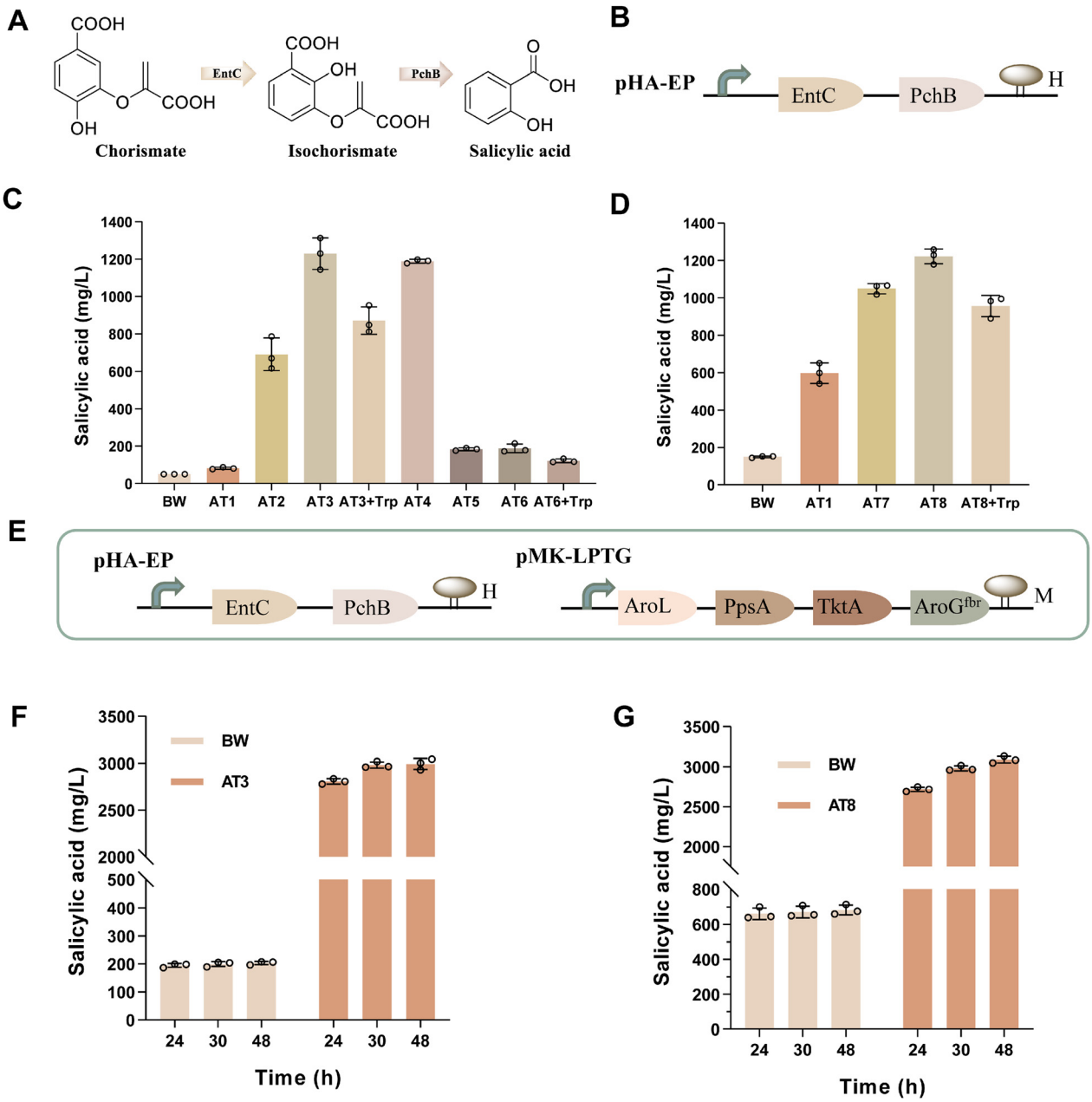

Fig. 3 Biosynthesis of SA through a pyruvate-based metabolic driving. (A) Schematic representation of the SA biosynthesis pathway. (B) Genes organization of pHA-EP. (C) Titer of SA achieved by glucose strains harbouring pHA-EP. (D) Titer of SA achieved by glycerol strains harbouring pHA-EP. (E) Genes organization of pHA-EP and pMK-LPTG. (F) Production of SA by BW25113 (F′) and AT3 using pHA-EP and pMK-LPTG. (G) Production of SA by BW25113 (F′) and AT8 using pHA-EP and pMK-LPTG. All data points are reported as mean ± standard deviation from three replicates.

strains. Based on their superior SA titers, AT3 (glucose-utilizing) and AT8 (glycerol-utilizing) were selected as host strains for subsequent *de novo* PA biosynthesis.

De novo PA production

Having established efficient SA biosynthesis and validated the PA-producing enzymes, we assembled the complete PA biosynthetic pathway by introducing three plasmids, pHA-EP, pMK-LPTG, and pLC-NahG-CbzE (a low-copy plasmid expressing nahG and cbzE in a single operon), into the host strain AT3, generating the engineered strain PAAT3-1 (Fig. 4A and B). Under initial cultivation conditions at 30 °C, PAAT3-1 produced 267.22 ± 3.87 mg L^{-1} PA from glucose after 48 h (Fig. 4C). Because 37 °C is the optimal growth temperature for *E. coli*, we also evaluated PA production at this temperature. PA accumulation increased to 314.23 ± 7.06 mg L^{-1} at 37 °C, representing a 1.18-fold improvement over the titer obtained at 30 °C (Fig. 4C).

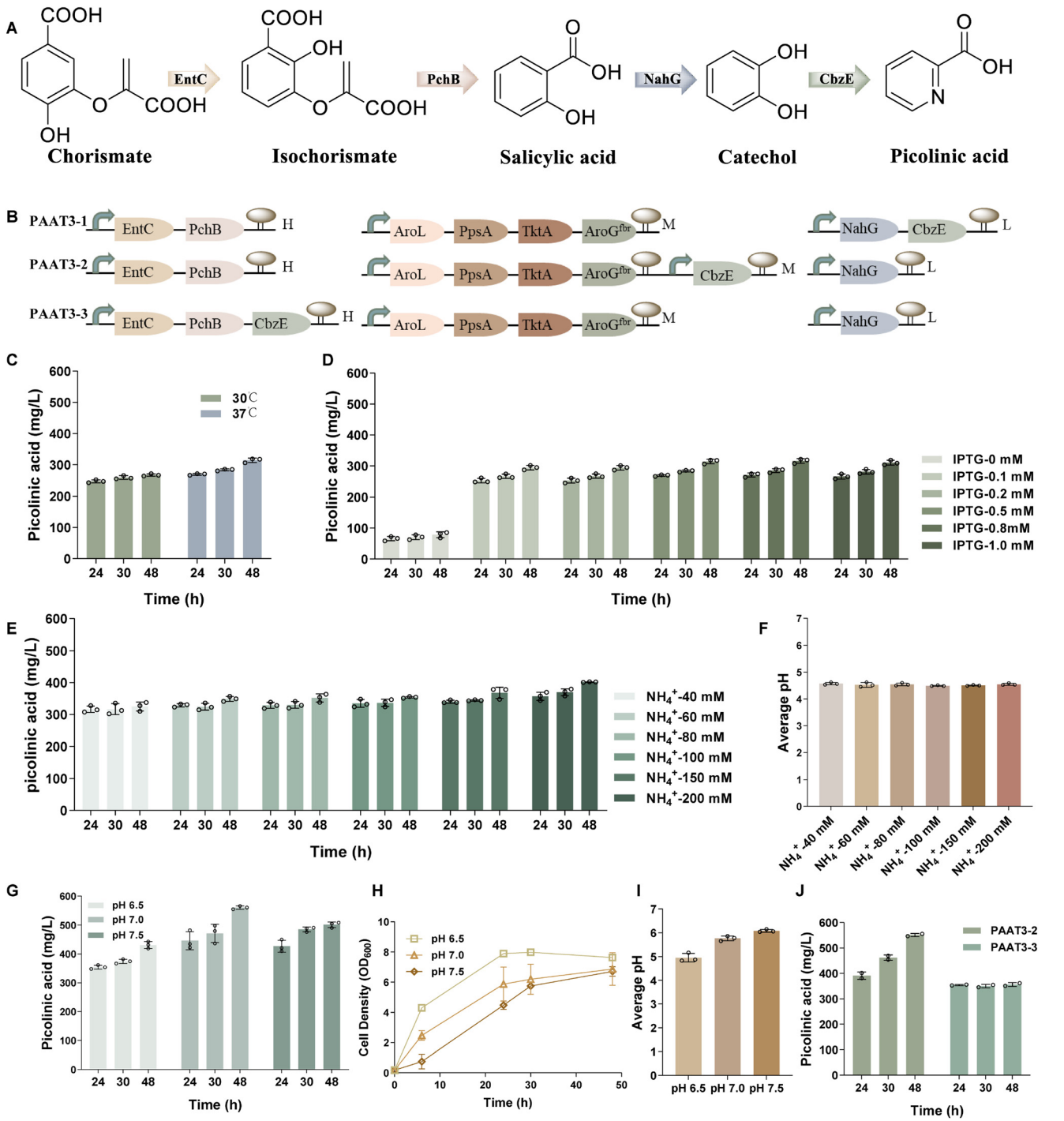

Fig. 4 *De novo* biosynthesis of PA and their optimizations in shake flask. (A) Non-natural PA pathway catalyzed by NahG and CbzE. (B) Illustration of plasmid constructs used for PA-producing strains. (C) PA titers of strain PAAT3-1 at different temperatures (30 and 37 °C). (D) PA titers of strain PAAT3-1 at different IPTG concentrations (0, 0.1, 0.2, 0.5, 0.8, and 1.0 mM). (E) PA titers of strain PAAT3-1 at different ammonium concentrations (40, 60, 80, 100, 150, and 200 mM). (F) Average pH of the shake flask cultures for PAAT3-1 at different ammonium concentrations. (G) PA titers of strain PAAT3-1 at different pH (6.5, 7.0, and 7.5). (H) OD_{600} of PAAT3-1 at different medium pH. (I) Average final pH of the shake flask cultures for PAAT3-1 at different initial pH. (J) PA titers of strains PAAT3-2 and PAAT3-3. All data points are reported as mean ± standard deviation from at least two replicates.

IPTG concentration strongly affects recombinant protein expression, with an optimal range required to balance sufficient induction against metabolic burden.[39] We therefore evaluated a series of IPTG concentrations (0, 0.1, 0.2, 0.5, 0.8, and 1.0 mM). The highest PA titer, 316.14 ± 7.57 mg L^{-1}, was obtained at 0.8 mM IPTG (Fig. 4D). Notably, PA titers remained comparably high across the 0.5–1.0 mM range, indicating that this interval represents the effective induction window for the pathway (Fig. 4D).

The terminal step in PA biosynthesis involves the spontaneous cyclization HMS, which requires the presence of ammonium to form the final product. To optimize PA yield, we investigated the influence of ammonium concentration across a range of 40–200 mM by supplementing the medium with $(NH_4)_2SO_4$. PA production increased progressively with ammonia concentration, reaching a maximum titer of 401.77 ± 1.00 mg L^{-1} at 200 mM, which corresponds to a 1.24-fold improvement over the titer obtained at 40 mM (325.31 ± 13.87 mg L^{-1}) (Fig. 4E).

Analysis of culture acidity revealed that the average pH of the cell culture dropped to approximately 4.5 after fermentation, a condition determined to be suboptimal and likely inhibitory for PA biosynthesis (Fig. 4F). Considering that *E. coli* is a neutralophile, we evaluated the effect of pH change by supplementing the medium with a stronger buffering system (2 g L^{-1} MOPS) and testing PA production with initial pH values of 6.5, 7.0, and 7.5. PA accumulation increased with pH increased from 6.5 to 7.0, reaching a maximum titer of 560.02 ± 5.75 mg L^{-1} with accumulation of catechol at 101.43 ± 64.31 mg L^{-1} (Fig. 4G and S3). Further increasing the pH to 7.5 led to a slight decrease in production (501.47 ± 9.63 mg L^{-1}), which correlated with a reduction in cell density (Fig. 4H). The use of buffering media effectively stabilized the culture, resulting in much less acidified fermentation broth (Fig. 4I). Moderate catechol accumulation was observed, likely due to oxygen limitation in shake flasks. CbzE is an extradiol catechol 2,3-dioxygenase that requires dissolved O_2 to cleave catechol to HMS; under O_2-limited conditions its turnover decreases, causing catechol to accumulate. We therefore anticipate that improved aeration will alleviate this bottleneck. For example, implementing fed-batch fermentation with increased aeration and agitation should maintain CbzE in an oxygen-saturated regime and minimize catechol buildup. Notably, catechol 2,3-dioxygenases from *Pseudomonas* strains isolated from hypoxic environments have evolved higher O_2 affinity to retain activity under low-oxygen conditions,[40] suggesting that ensuring sufficient O_2 supply or using a CbzE variant with enhanced O_2 affinity would alleviate catechol accumulation.

Enzyme expression level has significant impact in production efficiency. We therefore modulated CbzE expression by testing other two distinct plasmid configurations: (1) pHA-EP, pMK-LPTG-CbzE (a medium-copy-number plasmid co-expressing the LPTG and CbzE in two separate operons), and pLC-NahG; (2) pHA-EP-CbzE (a high-copy-number plasmid co-expressing the EP and CbzE in one operon), pMK-LPTG, and pLC-NahG. These plasmid sets were separately introduced into strain AT3, yielding the PA-producing strains PAAT3-2 and PAAT3-3 (Fig. 4B). After 48 h of cultivation, PAAT3-2 produced 551.01 ± 6.26 mg L^{-1} PA (Fig. 4J), a comparable to that of the original strain PAAT3-1, with no detectable catechol accumulation. In contrast, when CbzE was expressed from the high-copy-number plasmid in PAAT3-3, PA production dropped to 355.93 ± 7.50 mg L^{-1}, accompanied by substantial catechol accumulation (297.91 ± 13.52 mg L^{-1}) (Fig. S4). These results indicate that a relatively lower expression level of CbzE is more favourable for the performance of this artificial pathway. Additionally, no SA accumulation was detected during fermentation in all of strains.

When PA production was evaluated in glycerol-utilizing strains under the established optimal fermentation conditions and plasmid combination, PAAT8 accumulated only 355.33 ± 98.16 mg L^{-1} PA at 30 h, and the titer further declined to 227.91 ± 4.69 mg L^{-1} at 48 h (Fig. S5).

Conclusions

Conventional chemical synthesis of PA relies heavily on fossil-fuel-derived feedstocks and harsh oxidation chemistries (Fig. S6). Notably, ammoxidation of 2-picoline, as well as nitic acid or $KMnO_4$-based oxidation routes, are commonly employed, all of which generate substantial waste and raise environmental, safety, and occupational health concerns. For example, boiling alkaline $KMnO_4$ can oxidize picoline to PA, but this process requires hot caustic condition, extensive neutralization, and precipitation steps.[41] Another classical approach is the Lonza process, in which concentrated HNO_3 at 230–270 °C and 6–8 MPa oxidizes alkylpyridines to PA. While this nitric-acid oxidation gives high yields, it uses extremely corrosive, toxic reagents and releases large amounts of Nox, posing notable safety and environmental issues.[42]

In this work, we designed and implemented a rationally engineered artificial shortcut pathway for microbial PA production from renewable carbon sources using a retro-biosynthetic strategy. The constructed route integrates a hybrid SA biosynthetic module with a partial SA degradation pathway, involving only four enzymatic steps and shortening the natural biosynthetic sequence by seven steps.

Through enzyme validation, modular pathway assembly, enhancement of precursor supply, and optimization of cultivation conditions, we achieved efficient *de novo* PA biosynthesis, reaching a titer of 560.02 ± 5.75 mg L^{-1} in shake-flask cultures using glucose as the carbon source. This artificial pathway effectively circumvents the complexity, regulatory constraints, and low PA yield inherent in the natural kynurenine route.

Overall, this work demonstrates a promising biotechnological alternative to traditional chemical synthesis, offering a greener, safer, and more sustainable strategy for PA manufacturing. With further strain engineering and bioprocess optimization, this platform has strong potential to achieve the economic viability and commercial scalability required for industrial deployment.

Author contributions

Cui Guo conceived the project, performed the experiment, analyzed the data, and wrote the manuscript; Ashley Tseng performed the experiment and analyzed the data; Nguyen N. T. Luu performed the experiment and analyzed the data;

Yuheng Lin, conceived and supervised the project, wrote and modified the manuscript.

Conflicts of interest

A provisional patent related to this innovation is being filed by University of Houston.

Data availability

The data supporting this article have been included as part of the supplementary information (SI). Supplementary information is available. See DOI: https://doi.org/10.1039/d6gc00467a.

Acknowledgements

This work was supported by the Start-up Funds to Yuheng Lin from the Department of Engineering Technology, Cullen College of Engineering, University of Houston, and USDA's Hispanic-serving Institutions (HSI) Education Grant (2023-77040-41264).

References

1 I. Davis, Y. Yang, D. Wherritt and A. Liu, *J. Biol. Chem.*, 2018, **293**, 9594–9603.
2 R. S. Grant, S. E. Coggan and G. A. Smythe, *Int. J. Tryptophan Res.*, 2009, **2**, 71–79.
3 U. Testa, F. Louache, M. Titeux, P. Thomopoulos and H. Rochant, *Br. J. Haematol.*, 1985, **60**, 491–502.
4 S. Premma and A. Pasupathy, *St. Joseph's College (Autonomous)*.
5 A. N. Paiva, J. G. d. Lima, A. C. Q. d. Medeiros, H. A. O. Figueiredo, R. L. d. Andrade, M. A. G. Ururahy, A. A. Rezende, J. Brandão-Neto and M. d. G. Almeida, *J. Trace Elem. Med. Biol.*, 2015, **32**, 66–72.
6 C. L. Broadhurst and P. Domenico, *Diabetes Technol. Ther.*, 2006, **8**, 677–687.
7 S. A. Barrie, J. V. Wright, J. E. Pizzorno, E. Kutter and P. C. Barron, *Agents Actions*, 1987, **21**, 223–228.
8 D. Skrajnowska and B. Bobrowska-Korczak, *Nutrients*, 2019, **11**, 2273.
9 F. Hajializadeh, H. Ghahri and A. Talebi, *Vet. Res. Forum*, 2017, **8**, 259–264.
10 K. Sahin, C. Orhan, O. Kucuk, M. Tuzcu, N. Sahin, I. H. Ozercan, S. Sylla, S. P. Ojalvo and J. R. Komorowski, *Food Chem.: Mol. Sci.*, 2022, **4**, 100081.
11 S. Cai, K. Sato, T. Shimizu, S. Yamabe, M. Hiraki, C. Sano and H. Tomioka, *J. Antimicrob. Chemother.*, 2006, **57**, 85–93.
12 R. Narayan, M. Sharma, R. Yadav, A. Biji, O. Khatun, S. Kaur, A. Kanojia, C. M. Joy, R. Rajmani, P. R. Sharma, S. Jeyasankar, P. Rani, R. K. Shandil, S. Narayanan, D. C. Rao, V. Satchidanandam, S. Das, R. Agarwal and S. Tripathi, *Cell Rep. Med.*, 2023, **4**, 101127.
13 E. Al'kaeva, T. Andrushkevich, G. Zenkovets and D. J. C. L. Babushkin, *Catal. Lett.*, 1998, **54**, 149–152.
14 C. Guo, N. N. T. Luu, M. M. Adwer, H. Hosseinzadeh, V. Balan, Y. Yan and Y. Lin, *Metab. Eng.*, 2026, **94**, 24–34.
15 F. Hou, M. Xian and W. Huang, *Green Chem.*, 2021, **23**, 8280–8289.
16 Z.-F. Hu, A.-D. Gu, L. Liang, Y. Li, T. Gong, J.-J. Chen, T.-J. Chen, J.-L. Yang and P. Zhu, *Green Chem.*, 2019, **21**, 3286–3299.
17 J. Zhou, Z. Zhang, X. Xin, Y. Xue, Y. Wang, X. Feng, B. Zhang, M. Zhao, Z. Liu and Y. Zheng, *Green Chem.*, 2025, **27**, 1806–1819.
18 J. R. Moffett, P. Arun, N. Puthillathu, R. Vengilote, J. A. Ives, A. A.-B. Badawy and A. M. Namboodiri, *Front. Immunol.*, 2020, **11**, 31.
19 Y. Jiang, B. Chen, C. Duan, B. Sun, J. Yang and S. Yang, *Appl. Environ. Microbiol.*, 2015, **81**, 2506–2514.
20 R. Pellicciari, P. Liscio, N. Giacchè, F. De Franco, A. Carotti, J. Robertson, L. Cialabrini, E. Katsyuba, N. Raffaelli and J. Auwerx, *J. Med. Chem.*, 2018, **61**, 745–759.
21 Y. Asano, Y. Yamamoto and H. Yamada, *Biosci., Biotechnol., Biochem.*, 1994, **58**, 2054–2056.
22 Y. Lin, X. Sun, Q. Yuan and Y. Yan, *Metab. Eng.*, 2014, **23**, 62–69.
23 A. E. Mars, J. Kingma, S. R. Kaschabek, W. Reineke and D. B. Janssen, *J. Bacteriol.*, 1999, **181**, 1309–1318.
24 A. Kita, S.-I. Kita, I. Fujisawa, K. Inaka, T. Ishida, K. Horiike, M. Nozaki and K. Miki, *Structure*, 1999, **7**, 25–34.
25 M. A. Miller and J. D. Lipscomb, *J. Biol. Chem.*, 1996, **271**, 5524–5535.
26 M. W. Vetting, L. P. Wackett, L. Que Jr., J. D. Lipscomb and D. H. Ohlendorf, *J. Bacteriol.*, 2004, **186**, 1945–1958.
27 P. Adewale, A. Lang, F. Huang, D. Zhu, J. Sun, M. Ngadi and T. C. Yang, *Sci. Rep.*, 2021, **11**, 23982.
28 A. K. Whiting, Y. R. Boldt, M. P. Hendrich, L. P. Wackett and L. Que Jr., *Biochemistry*, 1996, **35**, 160–170.
29 M. Kunze, K. F. Zerlin, A. Retzlaff, J. O. Pohl, E. Schmidt, D. B. Janssen, R. Vilchez-Vargas, D. H. Pieper and W. Reineke, *Microbiology*, 2009, **155**, 4069–4083.
30 J. Wang, R. Zhang, Y. Zhang, Y. Yang, Y. Lin and Y. Yan, *Metab. Eng.*, 2019, **55**, 191–200.
31 S. Noda, Y. Mori, R. Fujiwara, T. Shirai, T. Tanaka and A. Kondo, *Metab. Eng.*, 2021, **67**, 1–10.
32 S. Tanaka, X. Han and R. Kahmann, *Front. Plant Sci.*, 2015, **6**, 349.
33 E. Ponce, N. Flores, A. Martinez, F. Valle and F. Bolívar, *J. Bacteriol.*, 1995, **177**, 5719–5722.
34 J.-Y. Jeong, Y.-J. Kim, N. Cho, D. Shin, T.-W. Nam, S. Ryu and Y.-J. Seok, *J. Biol. Chem.*, 2004, **279**, 38513–38518.
35 K. Ohta, H. Hamasuna, J. Tsukamoto, M. Wakiyama, Y. Izumi and K. Harada, *J. Biosci. Bioeng.*, 2012, **113**, 608–610.

36 X. Ren, Y. Wei, H. Zhao, J. Shao, F. Zeng, Z. Wang and L. Li, *Front. Bioeng. Biotechnol.*, 2023, **11**, 1261832.
37 A. Satanowski, B. Dronsella, E. Noor, B. Vögeli, H. He, P. Wichmann, T. J. Erb, S. N. Lindner and A. Bar-Even, *Nat. Commun.*, 2020, **11**, 5812.
38 K. D. Brown, *Genetics*, 1968, **60**, 31–48.
39 M. Mühlmann, E. Forsten, S. Noack and J. Büchs, *Microb. Cell Fact.*, 2017, **16**, 220.
40 J. J. Kukor and R. H. Olsen, *Appl. Environ. Microbiol.*, 1996, **62**, 1728–1740.
41 D. Lisicki, D. Talik and B. Orlińska, *Catalysts*, 2023, **13**, 1271.
42 C. B. Biswell and W. V. Wirth, *US Pat.* 2109954, 1938.